Quantitative assessment of brain iron by R_2* relaxometry in patients with clinically isolated syndrome and relapsing–remitting multiple sclerosis

M Khalil, C Enzinger, C Langkammer, M Tscherner, M Wallner-Blazek, M Jehna, S Ropele, S Fuchs and F Fazekas

Background Increased iron deposition has been implicated in the pathophysiology of multiple sclerosis (MS), based on visual analysis of signal reduction on T_2-weighted images. R_2* relaxometry allows to assess brain iron accumulation quantitatively.

Objective To investigate regional brain iron deposition in patients with a clinically isolated syndrome (CIS) or relapsing–remitting MS (RRMS) and its associations with demographical, clinical, and conventional magnetic resonance imaging (MRI) parameters.

Methods We studied 69 patients (CIS, $n = 32$; RRMS, $n = 37$) with 3T MRI and analyzed regional R_2* relaxation rates and their correlations with age, disease duration, disability, T_2 lesion load, and normalized brain volumes.

Results Basal ganglia R_2* relaxation rates increased in parallel with age ($r = 0.3$–0.6; $P < 0.01$) and were significantly higher in RRMS than in CIS ($P < 0.05$). Using multivariate linear regression analysis, the rate of putaminal iron deposition was independently predicted by the patients' age, disease duration, and gray matter atrophy.

Conclusions Quantitative assessment by R_2* relaxometry suggests increased iron deposition in the basal ganglia of MS patients, which is associated with disease duration and brain atrophy. This technique together with long-term follow-up thus appears suited to clarify whether regional iron accumulation contributes to MS morbidity or merely reflects an epiphenomenon. *Multiple Sclerosis* 2009; **15:** 1048–1054. http://msj.sagepub.com

Key words: 3T MRI; brain atrophy; deep gray matter; iron deposition; multiple sclerosis; R_2* mapping

Introduction

With normal aging, regions of the brain, particularly the basal ganglia, tend to accumulate nonhemin iron, primarily in the form of ferritin. Ferritin is a storage protein that contains up to 5000 ferric (Fe3+) ions and does not cross the blood–brain barrier. Abnormal iron deposition in the brain has been implicated in the pathophysiology of various neurodegenerative CNS disorders [1]. Although iron is essential for normal neuronal metabolism, excessive iron levels can exert neurotoxic effects by the formation of free radicals [2,3]. From several observations, excessive iron deposition has also been proposed to play a role in multiple sclerosis (MS).

Drayer [4] and Grimaud [5] were the first to report on a regionally specific signal reduction on T_2-weighted brain magnetic resonance imaging (MRI) images in MS, which was believed to indicate increased iron deposition. Bakshi *et al*. analyzed in more detail the frequency, location, and clinical significance of T_2 shortening in a larger cohort of MS patients [6]. In this study, T_2 hypointensity was found to be more pronounced in the thalamus, putamen, caudate nuclei, and in the rolandic cortex, and moreover to be associated with advanced disability. Further studies of this group, linked gray

Department of Neurology and Department of Radiology (Division of Neuroradiology), Medical University of Graz, Graz, Austria
Correspondence to: Franz Fazekas, MD, Department of Neurology, Medical University of Graz, Graz, Austria.
Email: franz.fazekas@medunigraz.at
Received 11 January 2009; accepted 26 April 2009

10.1177/1352458509106609

matter T_2 shortening to brain atrophy [7,8] and cognitive impairment [9]. The authors also suggested that gray matter T_2 shortening predicted the evolution of brain atrophy in untreated relapsing–remitting MS (RRMS) patients [10]. Altogether, these data give further credence to a possible pathophysiologic role of iron in MS. Although early investigations in this direction suffered from the methodological drawback of deducing iron concentrations from a visual grading of the reduction of signal intensity on T_2-weighted images, more recent studies have documented the extent of T_2 hypointensity in a quantitative manner [9–11]. The use of specific MRI sequences at higher (≥3T) field strengths may serve to further increase the sensitivity of depicting iron-related signal changes in the brain. This comes from the fact that the very densely packed ferric ions that are present in ferritin cause local changes of the magnetic susceptibility [12,13]. As a consequence, the water molecules surrounding the ferritin core experience a higher magnetic field and, thus, a shortening of the relaxation times when diffusing through the local field gradients. These effects become increasingly apparent with higher field strengths. Also, iron is detectable especially when it provokes a paramagnetic effect occurring with a mineralized state such as in the form of ferritin and hemosiderin. Current approaches to assess brain iron in a more quantitative manner are, therefore, based either on susceptometry or on relaxation time mapping, or they focus on a combined approach such as the magnetic field correlation (MFC) technique [14].

R_2* relaxation rate mapping is among the interesting candidates for iron mapping. On the basis of a gradient echo sequence with multiple echoes, this technique is readily available on modern MRI scanners. Provided a reasonable number of echoes and adequate handling of macroscopic susceptibility effects, robust R_2* maps can be obtained within a clinically acceptable acquisition time. We therefore decided to use this technique in a larger series of patients with a clinically isolated syndrome (CIS) or RRMS to search for differences in regional brain iron concentrations and to use it to reassess the suggested associations of iron deposition with clinical and morphologic features of the disease.

Patients and methods

Study participants were prospectively enrolled from our MS outpatient department. Inclusion criteria were a diagnosis of a CIS [15] or of a RRMS [16], regular follow-up visits and the patients' willingness, capacity and consent to undergo detailed clinical testing, and a comprehensive 3T MRI examination. Demographical and clinical data recorded included age, gender, age at disease onset, disease duration, and treatment. Disability was measured with the Expanded Disability Status Scale (EDSS) [17]. From the documented relapses, we calculated the annualized relapse rate as a measure of clinical disease activity. Relapses were defined as the appearance or reappearance of at least one neurological symptom or as the worsening of an old symptom attributed to MS that lasted for at least 24 h and was preceded by a relatively stable or improving neurological state of at least 30 days.

In all, 32 patients with a CIS and 37 with RRMS fulfilled these criteria and contributed to the analysis (for demographical and clinical data, see Table 1). A total of 6 CIS patients received interferon-β therapy. Of the 21 treated RRMS patients, 14 received interferon-β, 4 glatiramer acetate, 2 natalizumab, and 1 intravenous immunoglobulins.

Magnetic resonance imaging

Patients underwent MRI on a 3 Tesla system (Siemens Tim Trio, Siemens Medical Systems, Erlangen, Germany) using a 12-element receiver coil. Structural imaging included a fast Fluid attenuated inversion recovery (FLAIR) sequence (TR/TE/TI = 9000/70 ms/

Table 1 Clinical and demographical data

	All Patients	Patient Subgroups		
		CIS	RRMS	*P* Value
N (% female)	69 (63.8)	32 (68.8)	37 (59.5)	n.s.
Age[a] (years)	35.9 (26.7–41.4)	33.9 (24.8–39.9)	37.1 (32.1–42.4)	n.s.
Age at disease onset[a] (years)	28.6 (22.2–37.9)	33.6 (24.6–39.1)	25.6 (20.7–35.5)	<0.05
Disease duration[a] (years)	2.7 (0.3–10.4)	0.3 (0.1–0.9)	8.1 (4.2–13.3)	<0.001
Annualized relapse rate[a]	NA	NA	0.5 (0.2–1.1)	NA
EDSS[a]	2.0 (1.0–2.5)	1.0 (0.0–2.4)	2.0 (1.0–3.4)	<0.05
N treated patients (%)	27 (39.1)	6 (18.8)	21 (56.8)	<0.005

CIS, clinically isolated syndrome; RRMS, relapsing–remitting multiple sclerosis; N, number of patients; n.s., statistically not significant ($P > 0.05$); NA, not applicable; EDSS, Expanded Disability Status Scale [17].
[a]Median (interquartile range).

2500 ms, in plane resolution = 0.9 × 0.9 mm^2, slice thickness = 3 mm) and a T_1-weighted 3D Magnetization Prepared Rapid Acquisition Gradient Echo (MPRAGE) sequence with 1 mm isotropic resolution (TR/TE/TI/FA = 1.9 s/2.19 ms/0.9s/9°). For R_2* mapping, a spoiled 3D Fast Low Angle Shot (FLASH) sequence (TR/FA = 86 ms/20°) with 12 equally spaced echoes (bipolar readout gradient with echo spacing of 4.92 ms, in plane resolution = 0.9 × 0.9 mm^2, slice thickness = 4 mm, whole brain coverage) was used.

Image analysis

All image analyses were performed by trained and experienced technicians and interpreters, blinded to clinical information.

Regional R_2 mapping*

To eliminate image shifts caused by the bipolar data acquisition, all subsequent echoes provided by the FLASH sequence were registered with the first echo. Then, R_2* maps were calculated voxelwise by fitting a single exponential decay curve and by considering the contribution of non-Gaussian image noise with a least square approach proposed by St Pierre [18] and described in detail by St Pierre *et al*. [19] and He *et al*. [20].

On the basis of high-resolution MPRAGE scan, seven deep gray matter structures (thalamus, caudate nuclei, putamen, pallidum, hippocampus, amygdale, and nucleus accumbens) and the brainstem were segmented fully automatically for all subjects using FIRST, which is a segmentation and registration algorithm based on deformable models from FSL [21]. The resulting masks of these structures were eroded by 1 pixel to avoid overlapping with adjacent regions and used to define these regions in the fit R_2* data sets. Then, mean R_2* values and standard deviations were calculated for each structure by masking the R_2* maps and by averaging the values from both hemispheres. A representative R_2* map of the putamen, based on a 3T MRI is shown in Figure 1.

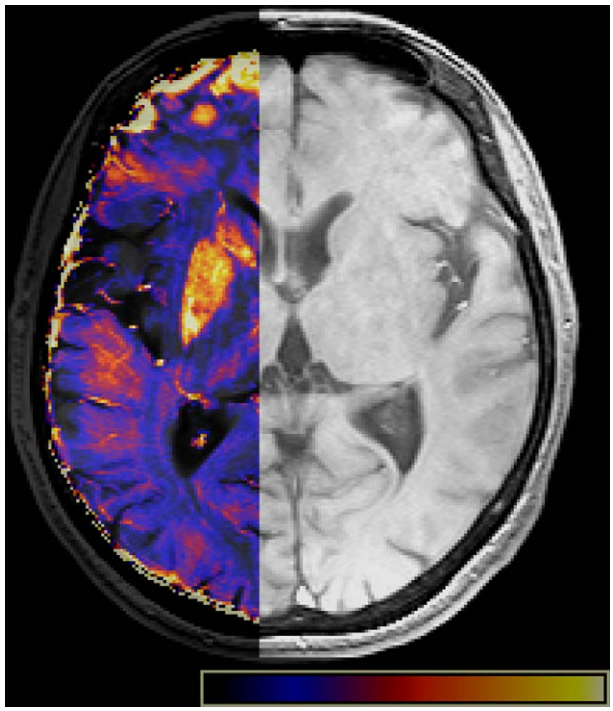

Figure 1 R_2* mapping. The first echo of the multiecho FLASH series and the corresponding R_2* map (overlay) is shown. The higher R_2* in the putamen reflects a higher iron load.

Atrophy

Brain tissue volume, normalized for subject head size, was estimated using SIENAX [22,23], part of FSL [21]. SIENAX starts by extracting brain and skull images from the single whole-head input data [24]. The brain image is then affine-registered to MNI152 space [25,26] (using the skull image to determine the registration scaling); this is done primarily to obtain the volumetric scaling factor to be used as normalization for head size. Next, tissue-type segmentation with partial volume estimation is carried out [27] to calculate the total volume of brain tissue (including separate estimates of volumes of gray matter, white matter, peripheral gray matter, and ventricular CSF).

Lesion load

MS lesions were outlined on a transparency overlaid on hard copies of the FLAIR sequence. Using these templates, lesion masks were then created using the DISPImage programme [28]. The lesion load was calculated by multiplying the area of all masks by the slice thickness.

Statistical analysis

Statistical analyses were performed using SPSS 15.0 (SPSS Inc., Chicago, Illinois, USA). Distribution of data was tested by the Kolmogorov–Smirnov test. Comparisons between groups were performed by Mann–Whitney *U* test or *t* test according to the statistical distribution of the data. In the combined patient

Table 2 Regional brain R_2* relaxation rates

	All Patients	Patient Subgroups		
		CIS	RRMS	*P* Value
Pallidum	34.2 (2.8)	33.0 (2.9)	35.2 (2.3)	<0.005
Putamen	26.0 (3.1)	24.7 (2.7)	27.2 (3.0)	<0.001
Caudate nuclei	24.6 (2.9)	23.6 (2.7)	25.4 (2.8)	<0.05
Thalamus	20.5 (1.1)	20.3 (1.1)	20.6 (1.1)	n.s.
Amygdala	32.8 (9.1)	34.6 (9.7)	31.3 (8.4)	n.s.
Nucleus accumbens	42.9 (11.2)	43.3 (11.3)	42.6 (11.2)	n.s.
Hippocampus	24.2 (4.9)	24.9 (5.7)	23.6 (4.1)	n.s.
Brain stem	21.2 (5.0)	22.1 (5.8)	20.5 (4.2)	n.s.

CIS, clinically isolated syndrome; RRMS, relapsing–remitting multiple sclerosis; n.s., statistically not significant ($P > 0.05$).
R_2* rates [s^{-1}] are given as mean (standard deviation).

groups, Spearman and Pearson correlations were performed to calculate the correlation coefficients between the imaging and the clinical data. Multivariate linear regression models were applied to identify the factors predicting R_2* changes and volumetric data. All regression models were controlled for age.

Results

Automatic measurement of R_2* in seven deep and cortical gray matter structures and the brainstem in our cohort yielded no significant difference between the left versus the right hemispheric R_2* rates in the respective brain regions. The mean and standard deviations of averaged values for both hemispheres are given in Table 2. As can be seen, there was evidence for a significantly higher iron accumulation in the basal ganglia, including putamen, pallidum, and caudate nuclei, in patients with RRMS compared to those with a CIS (Table 2).

Because of evidence that iron deposition may be more extensive in men than in premenopausal women of comparable age, we also performed separate analyses for both sexes. The results showed higher R_2* values in the basal ganglia of both male and female patients with RRMS compared to those with CIS (data not shown) but more robust differences in males. Given the relatively small patient numbers for these subanalyses, this finding will have to be confirmed in a larger patient cohort.

No significant differences were seen in the other brain regions analyzed.

CIS and RRMS patients differed regarding other MRI metrics (Table 3) including lesion load and several measures of brain atrophy (whole brain, whole gray matter, and cortex and ventricular volumes). As expected, T_2 lesion volume and brain atrophy were significantly more pronounced in RRMS compared to CIS patients (Table 3). No significant differences between CIS and RRMS were found in regard to white matter atrophy.

When assessing correlations of R_2* relaxation rates with demographic and clinical variables of both patient groups combined, we found a strong increase with age. This effect was most apparent in the putamen ($r = 0.6$; $P < 0.001$) (Figure 2), globus pallidus ($r = 0.5$; $P < 0.001$), and the caudate nuclei ($r = 0.3$; $P < 0.01$). Longer disease duration correlated with higher iron levels in the putamen ($r = 0.5$; $P < 0.001$), globus pallidus ($r = 0.4$; $P < 0.001$), and the caudate nuclei ($r = 0.3$; $P < 0.005$). No significant correlations were found between the EDSS and the R_2* relaxation rates.

Volumes of whole brain, whole gray matter, and cortex correlated negatively with R_2* relaxation rates in the putamen ($r = -0.5$ to -0.6; $P < 0.001$),

Table 3 Morphological data

	All Patients	Patient Subgroups		
		CIS	RRMS	*P* Value
Brain volume, cm^3	1604.2 (87.9)	1643.7 (66.3)	1571.1 (90.8)	<0.001
Gray matter volume, cm^3	851.9 (73.7)	883.4 (50.5)	825.4 (80.1)	<0.005
Cortex volume, cm^3	697.0 (57.5)	724.2 (44.8)	674.2 (57.7)	<0.001
White matter volume, cm^3	752.3 (49.6)	760.3 (56.0)	745.6 (43.2)	n.s.
Ventricular volume, cm^3	37.1 (21.8)	28.0 (14.0)	44.8 (24.2)	<0.005
Lesion load[a], cm^3	10.0 (3.0–24.0)	4.1 (1.9–11.8)	17.6 (7.3–31.2)	<0.001

CIS, clinically isolated syndrome; RRMS, relapsing–remitting MS; n.s., statistically not significant ($P > 0.05$).
Values are given as mean (standard deviation) or as [a]median (interquartile range).

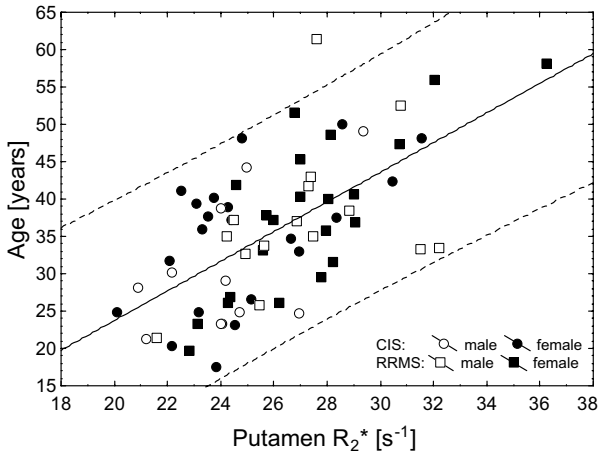

Figure 2 Graph showing the correlation of putaminal R_2* relaxation rates with increasing age ($r = 0.6$; $P < 0.001$).

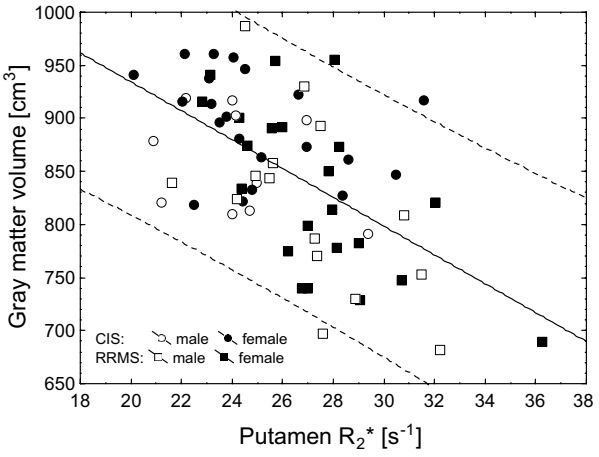

Figure 3 Graph showing the correlation of putaminal R_2* relaxation rates with whole gray matter atrophy. Reduced gray matter volumes are associated with higher putaminal iron levels measured by R_2* relaxometry ($r = -0.6$; $P < 0.001$).

globus pallidus ($r = -0.5$ to -0.6; $P < 0.001$), and the caudate nuclei ($r = -0.3$; $P < 0.05$) while ventricular volumes correlated positively with R_2* relaxometry measures in the putamen ($r = 0.5$; $P < 0.001$), globus pallidus (r = 0.4; $P < 0.005$), and the caudate nuclei ($r = 0.3$; $P < 0.05$). Figure 3 shows the correlation of putaminal iron levels with gray matter atrophy ($r = -0.6$; $P < 0.001$). Increased lesion load was associated with higher R_2* relaxation rates in the putamen ($r = 0.4$; $P = 0.001$) and globus pallidus ($r = 0.5$; $P < 0.001$).

Using a multivariate linear regression model, putaminal R_2* relaxation rates were independently predicted by age, disease duration, and gray matter atrophy (Table 4). EDSS and the annualized relapse rate did not enter this model. Accordingly, when assessing predictors of gray matter atrophy, we used linear regression analysis to identify lesion load and iron deposition in the putamen as independent variables (Table 4).

Discussion

This study provides a strong quantitative confirmation of earlier reports on increased iron levels with advancing stages of MS [4,7,29,30]. R_2* relaxation rates in the putamen, globus pallidus, and the caudate nuclei were significantly increased in RRMS compared to CIS. Furthermore, disease duration was identified as an independent predictor of the extent of putaminal iron accumulation. This is in line with earlier studies that estimated brain iron levels from visual interpretation of the T_2 signal reduction [6] and with a most recent investigation performed at 7T [30]. In this investigation, high-resolution gradient-echo phase images for quantification of local field shifts were used to show pathologically increased iron deposition in the basal ganglia of MS patients, which was associated

Table 4 Multivariate linear regression model

Dependent Variable	Independent Variable	Beta	Rho	*P* Value
R_2* putamen	Age (years)	0.4	0.6	<0.001
	Disease duration (years)	0.2	0.5	<0.05
	Gray matter volume (cm^3)	−0.3	−0.6	<0.05
	Lesion load (cm^3)	−0.0	0.3	n.s.
Gray matter volume (cm^3)	Age (years)	−0.2	−0.5	n.s.
	R_2* putamen	−0.3	−0.6	<0.05
	Disease duration (years)	−0.2	−0.5	n.s.
	Lesion load (cm^3)	−0.3	−0.5	<0.05

n.s., statistically not significant.
All multivariate linear regression models were controlled for age. R_2* in the putamen was independently predicted by disease duration and gray matter atrophy. R_2* putamen and lesion load were identified as independent factors predicting gray matter atrophy.

with disease duration [30]. Because our patients' R_2* relaxation rates were not compared with those of healthy individuals, we cannot rule out that the R_2* relaxation rates in brain regions with no significant differences between CIS and RRMS are increased in MS patients. This needs to be investigated further.

Another major finding is the link between iron deposition and brain atrophy, which has been suggested earlier by correlations between T_2 hypointensity and brain atrophy [7,8,10] and which is now corroborated by our quantitative R_2* measurements. In this context, it is important to note that local R_2* changes do not only reflect changes in brain iron load. Other sources of local magnetic field gradients, for example, a higher density of venules or macroscopic susceptibility effects such as those observed at air-tissue boundaries, may also increase the apparent R_2* rate. However, provided appropriate shimming, R_2* can be expected to scale with the paramagnetic effect of highly ordered ferric ions [31]. R_2* is the fastest transverse relaxation rate and is the sum of R_2' and R_2. R_2' arises from the transverse relaxation mechanisms that reflect the reversible signal loss associated with the local field inhomogeneities while R_2 reflects the nonreversible relaxation effects. Therefore, R_2' is assumed to be the most sensitive relaxation parameter for iron deposition [32]. However, R_2' mapping would require simultaneous mapping of R_2* and R_2. The assessment of R_2 with a multiecho spin-echo sequence is time consuming and it is also limited by the specific absorption rate at 3 Tesla. Therefore, in this study, we used a gradient echo approach that allows fast whole brain R_2* mapping in only a few minutes. In addition, fitting a single exponential decay function into 12 echoes enables a robust estimation of T_2*.

Our quantitative approach identified age as an important factor of iron accumulation in the deep gray matter nuclei, especially the basal ganglia. This highlights the importance of considering age as a covariate in analyses of cerebral iron accumulation. In this context, it should be emphasized that, in our cohort, age was not significantly different between CIS and RRMS patients.

The exact underlying pathophysiological mechanism(s) leading to increased iron deposition in the deep gray matter areas and the implications of this finding are still a matter of debate. Iron deposits have been described in macrophages and reactive microglia of MS brain tissue [33], and increased CSF ferritin levels were reported in patients with progressive MS [34]. Increased iron levels can exert toxic effects by the formation of free radicals [3] and may subsequently lead to neurodegeneration [2].

Earlier reports described a relation between lesion volume and brain iron deposition based on iron detection by T_2 hypointensities [8] and MFC [29]. In contrast to these studies, we could not identify T_2 lesion volume as an independent factor influencing R_2* relaxometry rates although a significant linear correlation between R_2* relaxation rates in the putamen as well as globus pallidus and T_2 lesion volume was present.

We identified increased gray matter atrophy as an independent predictor of putaminal R_2* relaxation rates indicative of higher amounts of iron. Such an association was not found in respect to white matter atrophy. This suggests iron deposition to be related to the degenerative rather than the inflammatory components of MS, although one might also argue that a potential impact of cortical lesions was not sufficiently assessed with the applied techniques. From pathological data, however, we do not expect a high rate of cortical lesions in the investigated cohort.

MRI T_2 hypointensities of deep gray matter areas have previously been associated with advanced neurological disability [6,7,11]. In the currently published study by Hammond *et al*. local field shifts from iron at 7T did not correlate with advanced disability [30]. These findings are in line with the results of the current study where R_2* rates were not significantly associated with the EDSS. However, this does not necessarily contradict earlier findings, as we studied patients within a very small range of lower EDSS scores. Also, the deep gray matter nuclei may not be the most sensitive region for assessing correlations of iron deposition with disability. For this purpose, cortical measurements would be preferable but they are problematic for R_2* mapping due to macroscopic field gradients that occur at transitions between tissues with different magnetic susceptibility. As increased iron deposition has previously been linked to impaired cognitive performance [9,29], further studies are needed to investigate whether brain iron levels estimated by the current approach are related to cognitive impairment in MS patients.

Unfortunately, our study cannot serve to clarify whether the excess of iron in gray matter areas is a primary cause of tissue damage and neurodegeneration or merely an epiphenomenon of pathophysiological processes occurring during the progression of MS [14]. Nevertheless, our multiregional analysis indicates that iron accumulation with increasing MS duration does not occur in a diffuse manner but that the basal ganglia appear to be preferentially affected. Considering that the corticospinal tract traverses the basal ganglia, it is tempting to speculate that increasing rates of iron deposition could ultimately contribute to the chronic progressive phase of MS. The strong correlation between R_2* relaxation rates and age – apparently also a crucial factor for the onset of chronic progression – and the observed correlations with gray matter atrophy may

support this hypothesis. Clearly, this will require long-term follow-up studies and a more detailed regional analysis. As we have demonstrated, the R_2* relaxation technique can be a useful tool for such investigations.

References

1. Bartzokis, G, Tishler, TA, Shin, IS, Lu, PH, Cummings, JL. Brain ferritin iron as a risk factor for age at onset in neurodegenerative diseases. *Ann N Y Acad Sci* 2004; **1012**: 224–236.
2. Campbell, A, Smith, MA, Sayre, LM, Bondy, SC, Perry, G. Mechanisms by which metals promote events connected to neurodegenerative diseases. *Brain Res Bull* 2001; **55**: 125–132.
3. Gutteridge, JM. Iron and oxygen radicals in brain. *Ann Neurol* 1992; **32**(Suppl): S16–S21.
4. Drayer, B, Burger, P, Hurwitz, B, Dawson, D, Cain, J. Reduced signal intensity on MR images of thalamus and putamen in multiple sclerosis: increased iron content. *AJR Am J Roentgenol* 1987; **149**: 357–363.
5. Grimaud, J, Millar, J, Thorpe, JW, Moseley, IF, McDonald, WI, Miller, DH. Signal intensity on MRI of basal ganglia in multiple sclerosis. *J Neurol Neurosurg Psychiatry* 1995; **59**: 306–308.
6. Bakshi, R, Shaikh, ZA, Janardhan, V. MRI T2 shortening ('black T2') in multiple sclerosis: frequency, location, and clinical correlation. *Neuroreport* 2000; **11**: 15–21.
7. Bakshi, R, Benedict, RH, Bermel, RA, *et al*. T2 hypointensity in the deep gray matter of patients with multiple sclerosis: a quantitative magnetic resonance imaging study. *Arch Neurol* 2002; **59**: 62–68.
8. Bakshi, R, Dmochowski, J, Shaikh, ZA, Jacobs, L. Gray matter T2 hypointensity is related to plaques and atrophy in the brains of multiple sclerosis patients. *J Neurol Sci* 2001; **185**: 19–26.
9. Brass, SD, Benedict, RH, Weinstock-Guttman, B, Munschauer, F, Bakshi, R. Cognitive impairment is associated with subcortical magnetic resonance imaging grey matter T2 hypointensity in multiple sclerosis. *Mult Scler* 2006; **12**: 437–444.
10. Bermel, RA, Puli, SR, Rudick, RA, *et al*. Prediction of longitudinal brain atrophy in multiple sclerosis by gray matter magnetic resonance imaging T2 hypointensity. *Arch Neurol* 2005; **62**: 1371–1376.
11. Tjoa, CW, Benedict, RH, Weinstock-Guttman, B, Fabiano, AJ, Bakshi, R. MRI T2 hypointensity of the dentate nucleus is related to ambulatory impairment in multiple sclerosis. *J Neurol Sci* 2005; **234**: 17–24.
12. Haacke, EM, Cheng, NY, House, MJ, *et al*. Imaging iron stores in the brain using magnetic resonance imaging. *Magn Reson Imaging* 2005; **23**: 1–25.
13. Schenck, JF. Magnetic resonance imaging of brain iron. *J Neurol Sci* 2003; **207**: 99–102.
14. Stankiewicz, J, Panter, SS, Neema, M, Arora, A, Batt, CE, Bakshi, R. Iron in chronic brain disorders: imaging and neurotherapeutic implications. *Neurotherapeutics* 2007; **4**: 371–386.
15. Miller, D, Weinshenker, B, Filippi, M, *et al*. Differential diagnosis of suspected multiple sclerosis: a consensus approach. *Mult Scler* 2008; **14**: 1157–1174.
16. Polman, CH, Reingold, SC, Edan, G, *et al*. Diagnostic criteria for multiple sclerosis: 2005 revisions to the "McDonald Criteria". *Ann Neurol* 2005; **58**: 840–846.
17. Kurtzke, JF. Rating neurologic impairment in multiple sclerosis: an expanded disability status scale (EDSS). *Neurology* 1983; **33**: 1444–1452.
18. St Pierre, TG. Deferiprone versus desferrioxamine in thalassaemia, and T2* validation and utility. *Lancet* 2003; **361**: 182, author reply : 183–184.
19. St Pierre, TG, Clark, PR, Chua-Anusorn, W. Single spin-echo proton transverse relaxometry of iron-loaded liver. *NMR Biomed* 2004; **17**: 446–458.
20. He, T, Gatehouse, PD, Smith, GC, Mohiaddin, RH, Pennell, DJ, Firmin, DN. Myocardial T2* measurements in iron-overloaded thalassemia: an in vivo study to investigate optimal methods of quantification. *Magn Reson Med* 2008; **60**: 1082–1089.
21. Smith, SM, Jenkinson, M, Woolrich, MW, *et al*. Advances in functional and structural MR image analysis and implementation as FSL. *Neuroimage* 2004; **23**(Suppl. 1): S208–S219.
22. Smith, SM, De Stefano, N, Jenkinson, M, Matthews, PM. Normalized accurate measurement of longitudinal brain change. *J Comput Assist Tomogr* 2001; **25**: 466–475.
23. Smith, SM, Zhang, Y, Jenkinson, M, *et al*. Accurate, robust, and automated longitudinal and cross-sectional brain change analysis. *Neuroimage* 2002; **17**: 479–489.
24. Smith, SM. Fast robust automated brain extraction. *Hum Brain Mapp* 2002; **17**: 143–155.
25. Jenkinson, M, Bannister, P, Brady, M, Smith, S. Improved optimization for the robust and accurate linear registration and motion correction of brain images. *Neuroimage* 2002; **17**: 825–841.
26. Jenkinson, M, Smith, S. A global optimisation method for robust affine registration of brain images. *Med Image Anal* 2001; **5**: 143–156.
27. Zhang, Y, Brady, M, Smith, S. Segmentation of brain MR images through a hidden Markov random field model and the expectation-maximization algorithm. *IEEE Trans Med Imaging* 2001; **20**: 45–57.
28. Plummer, DL. Dispimage: a display and analysis tool for medical images. Rev Neuroradiol 1992; **5**: 489–495.
29. Ge, Y, Jensen, JH, Lu, H, *et al*. Quantitative assessment of iron accumulation in the deep gray matter of multiple sclerosis by magnetic field correlation imaging. *AJNR Am J Neuroradiol* 2007; **28**: 1639–1644.
30. Hammond, KE, Metcalf, M, Carvajal, L, *et al*. Quantitative in vivo magnetic resonance imaging of multiple sclerosis at 7 Tesla with sensitivity to iron. *Ann Neurol* 2008; **64**: 707–713.
31. Yao, B, Li, TQ, Gelderen, P, Shmueli, K, de Zwart, JA, Duyn, JH. Susceptibility contrast in high field MRI of human brain as a function of tissue iron content. *Neuroimage* 2009; **44**: 1259–1266.
32. Gelman, N, Gorell, JM, Barker, PB, *et al*. MR imaging of human brain at 3.0 T: preliminary report on transverse relaxation rates and relation to estimated iron content. *Radiology* 1999; **210**: 759–767.
33. LeVine, SM. Iron deposits in multiple sclerosis and Alzheimer's disease brains. *Brain Res* 1997; **760**: 298–303.
34. LeVine, SM, Lynch, SG, Ou, CN, Wulser, MJ, Tam, E, Boo, N. Ferritin, transferrin and iron concentrations in the cerebrospinal fluid of multiple sclerosis patients. *Brain Res* 1999; **821**: 511–515.